Depth-resolved imaging and detection of micro-retroreflectors within biological tissue using Optical Coherence Tomography

Steven N. Ivers,[1] Stephan A. Baranov,[1] Tim Sherlock,[2] Katerina Kourentzi,[3] Paul Ruchhoeft,[2] Richard Willson,[1,3] and Kirill V. Larin[1,2,4,*]

[1]*Department of Biomedical Engineering, University of Houston, N308Engineering Building 1,Houston, TX 77204, USA*
[2]*Department of Electrical and Computer Engineering, University of Houston, N308 Engineering Building 1, Houston, TX 77204, USA*
[3]*Department of Chemical and Biomolecular Engineering, University of Houston, S222Engineering Building 1, Houston, TX 77204, USA*
[4]*Institute of Optics and Biophotonics, Saratov State University, Saratov 410012, Russia*
**klarin@uh.edu*

Abstract: A new approach to *in vivo* biosensor design is introduced, based on the use of an implantable micron-sized retroreflector-based platform and non-invasive imaging of its surface reflectivity by Optical Coherence Tomography (OCT). The possibility of using OCT for the depth-resolved imaging and detection of micro-retroreflectors in highly turbid media, including tissue, is demonstrated. The maximum imaging depth for the detection of the micro-retroreflector-based platform within the surrounding media was found to be 0.91 mm for porcine tissue and 1.65 mm for whole milk. With further development, it may be possible to utilize OCT and micro-retroreflectors as a tool for continuous monitoring of analytes in the subcutaneous tissue.

OCIS codes: (110.4500) Optical coherence tomography; (170.4500) Optical coherence tomography; (170.4580) Optical diagnostics for medicine; (280.4788) Optical sensing and sensors.

References and links

1. M. J. Pelletier, *Analytical Applications Of Raman Spectroscopy* (Blackwell Science, 1999).
2. D. A. Stuart, C. R. Yonzon, X. Zhang, O. Lyandres, N. C. Shah, M. R. Glucksberg, J. T. Walsh, and R. P. Van Duyne, "Glucose sensing using near-infrared surface-enhanced Raman spectroscopy: gold surfaces, 10-day stability, and improved accuracy," Anal. Chem. **77**(13), 4013–4019 (2005).
3. D. A. Stuart, J. M. Yuen, N. Shah, O. Lyandres, C. R. Yonzon, M. R. Glucksberg, J. T. Walsh, and R. P. Van Duyne, "In vivo glucose measurement by surface-enhanced Raman spectroscopy," Anal. Chem. **78**(20), 7211–7215 (2006).
4. M. Kinnunen, R. Myllylä, T. Jokela, and S. Vainio, "In vitro studies toward noninvasive glucose monitoring with optical coherence tomography," Appl. Opt. **45**(10), 2251–2260 (2006).
5. R. O. Esenaliev, K. V. Larin, I. V. Larina, and M. Motamedi, "Noninvasive monitoring of glucose concentration with optical coherence tomography," Opt. Lett. **26**(13), 992–994 (2001).
6. D. C. Klonoff, "Continuous glucose monitoring: roadmap for 21st century diabetes therapy," Diabetes Care **28**(5), 1231–1239 (2005).
7. O. Lazcka, F. J. D. Campo, and F. X. Muñoz, "Pathogen detection: a perspective of traditional methods and biosensors," Biosens. Bioelectron. **22**(7), 1205–1217 (2007).
8. F. P. Mathew, and E. C. Alocilja, "Porous silicon-based biosensor for pathogen detection," Biosens. Bioelectron. **20**(8), 1656–1661 (2005).
9. G. Harwood, "Amperometric enzyme biosensors for the analysis of drugs and metabolites," Adv. Drug Deliv. Rev. **18**(2), 163–191 (1996).
10. M. A. Cooper, "Optical biosensors in drug discovery," Nat. Rev. Drug Discov. **1**(7), 515–528 (2002).

#130861 - $15.00 USD Received 29 Jun 2010; revised 23 Jul 2010; accepted 23 Jul 2010; published 2 Aug 2010

11. T. M. Anh, S. V. Dzyadevych, M. C. Van, N. J. Renault, C. N. Duc, and J. M. Chovelon, "Conductometric tyrosinase biosensor for the detection of diuron, atrazine and its main metabolites," Talanta **63**(2), 365–370 (2004).
12. D. G. Myszka, and R. L. Rich, "Implementing surface plasmon resonance biosensors in drug discovery," Pharm. Sci. Technol. Today **3**(9), 310–317 (2000).
13. "American Diabetes Association: clinical practice recommendations 1997," Diabetes Care **20**(Suppl 1), S1–S70 (1997).
14. G. L. Coté, "Noninvasive and minimally-invasive optical monitoring technologies," J. Nutr. **131**(5), 1596S–1604S (2001).
15. L. J. McCartney, J. C. Pickup, O. J. Rolinski, and D. J. Birch, "Near-infrared fluorescence lifetime assay for serum glucose based on allophycocyanin-labeled concanavalin A," Anal. Biochem. **292**(2), 216–221 (2001).
16. R. Ballerstadt, A. Gowda, and R. McNichols, "Fluorescence resonance energy transfer-based near-infrared fluorescence sensor for glucose monitoring," Diabetes Technol. Ther. **6**(2), 191–200 (2004).
17. V. Handerek, H. Mcardle, T. Willats, N. Psaila, and L. Laycock, "Experimental retroreflectors with very wide field of view," in Proceedings of SPIE, the International Society for Optical Engineering 598611.1–598611.7 (2005).
18. R. Hodgson, and R. Chipman, "Measurement of corner-cube polarization," in *Polarimetry: Radar, Infrared, Visible, Ultraviolet, And X-Ray* (SPIE, 1990).
19. R. Nilsen, and X. Lu, "Retroreflection technology in Optics and Photonics for Counterterrorism and Crime Fighting," in *SPIE* (2004).
20. Y. Sheng, and H. H. Arsenault, "Corner-cube array for integrated optoelectronic cellular array interconnections," in *Digital Optical Computing II*, R. Arrathoon (SPIE, 1990), pp. 123–130.
21. M. L. Biermann, W. S. Rabinovich, R. Mahon, and G. C. Gilbreath, "Design and analysis of a diffraction-limited cat's-eye retroreflector," Opt. Eng. **41**(7), 1655–1660 (2002).
22. T. Takatsuji, M. Goto, S. Osawa, R. Yin, and T. Kurosawa, "Whole-viewing-angle cat's-eye retroreflector as a target of laser trackers," Meas. Sci. Technol. **10**(87–N), 90 (1999).
23. D. Huang, E. A. Swanson, C. P. Lin, J. S. Schuman, W. G. Stinson, W. Chang, M. R. Hee, T. Flotte, K. Gregory, C. A. Puliafito, and et, "Optical coherence tomography," Science **254**(5035), 1178–1181 (1991).
24. A. J. Jääskeläinen, K. E. Peiponen, and J. A. Räty, "On reflectometric measurement of a refractive index of milk," J. Dairy Sci. **84**(1), 38–43 (2001).
25. C. Drew, and C. Rylander, "Mechanical compression for dehydration and optical clearing of skin," in *Proceedings Of ASME 2008 Summer Bioengineering Conference* (2008).
26. Y. He, and R. K. Wang, "Dynamic optical clearing effect of tissue impregnated with hyperosmotic agents and studied with optical coherence tomography," J. Biomed. Opt. **9**(1), 200–206 (2004).
27. J. M. Schmitt, and G. Kumar, "Optical scattering properties of soft tissue: a discrete particle model," Appl. Opt. **37**(13), 2788–2797 (1998).
28. J. M. Schmitt, and G. Kumar, "Turbulent nature of refractive-index variations in biological tissue," Opt. Lett. **21**(16), 1310–1312 (1996).

1. Introduction

A broad range of biosensors are used today in clinical applications, ranging from glucose monitoring in diabetic patients [1–6], to pathogen detection [7,8], and to drug and toxic metabolite detection in tissues [9–12]. Most applications do not require recurrent monitoring of specific analytes, and these measurements can be performed *in vitro*. However for monitoring of, e.g., glucose levels, it is desirable to make frequent (or even continuous) measurements. A practice recommended by the American Diabetes Association for diabetic patient evaluation is to monitor blood glucose levels 3-4 times daily for type I diabetics and once each day for type II diabetics [13]. Such monitoring can be difficult and uncomfortable for the patient because most methods for monitoring blood glucose levels require puncturing of the skin. Thus, it is important to develop alternate approaches that would make it easier and less painful for patients to monitor frequently their vital analytes.

Usually, biosensors require contact between an analyte-sensitive biological element and the tissue for the creation of a measurable signal. The development of *implantable* biosensors can avoid the aforementioned disadvantage of skin puncturing by providing potentially non-invasive monitoring of the analyte of interest. A sub-millimeter-sized implantable biosensor platform can be placed within the hypodermis (the subcutaneous tissue), which would minimize the discomfort associated with daily readings. Utilizing such small implantable biosensors in the subcutaneous tissue would allow access to the dermis and sub-dermis tissue layers, which contain many analytes of interest (e.g., glucose).

#130861 - $15.00 USD Received 29 Jun 2010; revised 23 Jul 2010; accepted 23 Jul 2010; published 2 Aug 2010

For glucose monitoring, many research efforts have been focused on the Concanavalin A (ConA)-dextran system which, unlike glucose-oxidase-based sensors, is independent of local oxygen levels [14–16]. For our envisioned retroreflector-based biosensor, we plan to immobilize ConA or other glucose binding agents, such as boronate, onto the implantable biosensor surface and allow dextran-coated gold nanoparticles to assemble onto the biosensor surface. The presence of glucose will induce the dissociation of the dextran-coated gold nanoparticles from the ConA-coated surface and increase reflectivity of the surface. More importantly, changes in glucose levels will induce changes in the reflectivity of the biosensor surface due to the light scattering caused by the presence of gold nanoparticles. In this approach, an imaging technique must be used that is capable of resolving retroreflectors implanted in subcutaneous tissue, and reliably measuring the *reflectivity* of the biosensor surface, which signals the glucose concentration.

Towards this goal, we have recently developed a highly reflective, micro-retroreflector-based substrate as a platform for the biosensor. This design includes an array of micron-sized retroreflectors (micro-retroreflectors) fabricated on a silicon substrate. Retroreflectors are unlike planar mirrors, which only return maximum light directly back to the source if the mirror is perpendicular to the wave front. In contrast, retroreflectors reflect incident light in an anti-parallel manner directly back to its source for a wide range of angles without the need for precise alignment. Retroreflectors exist in the form of linear retroreflectors, prisms (or corner cubes), spheres, and cat's eye retroreflectors [17–22], most of which have to date only been fabricated in the form of reflective sheets for use in road signs, vehicle reflectors, and safety clothing. For this study, simple linear *micro*-retroreflectors were used, as schematically shown in Fig. 1.

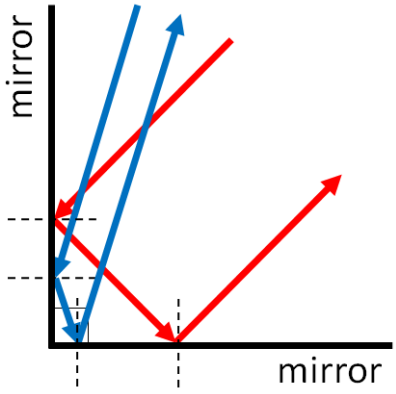

Fig. 1. Linear micro-retroreflector: two reflecting surfaces where incident light is always directed back to the source in an anti-parallel manner.

Development of the biosensor platform requires an imaging technique capable of receiving depth-resolved reflections from the micro-retroreflector-based platform surface as well as achieving high spatial resolution for detection of multiple micro-retroreflectors in tissue. Conventional imaging modalities such as magnetic resonance imaging, ultrasound, and X-ray imaging are capable of imaging structures within tissue, but these modalities lack the high spatial resolution and/or potential analyte-responsiveness required for our application of detecting micro-retroreflectors within tissue.

In this study, therefore, we investigated the use of Optical Coherence Tomography (OCT) [23], a non-invasive and depth-resolved imaging technique, for reflectance measurements of micro-retroreflectors in the subcutaneous tissue. OCT has high transverse resolution (<10 μm), which allows for the visualization of individual micro-retroreflectors in tissue, high SNR (up to 120 dB) for the precise detection of optical signals when returning from tissue, high in-depth resolution (~10 μm), and several millimeters of depth penetration in order to image

#130861 - $15.00 USD Received 29 Jun 2010; revised 23 Jul 2010; accepted 23 Jul 2010; published 2 Aug 2010

through the *stratum corneum* and epidermis layers of the skin. In conventional OCT, a two-beam interferometer is used to obtain depth-profiled information on the sample of interest within the coherence length of the laser. A beam from a broadband low-coherence laser source is split into the reference and sample arms of the interferometer. The backscattered light from the sample is recombined with the back-reflected light from the reference arm, resulting in the formation of interference fringes, which are captured by an optical sensor. OCT methods can be divided into two classes, Time Domain (TD-OCT) and Fourier Domain (FD-OCT), which is further split into Swept Source OCT (SS-OCT) and Spectral Domain OCT (SD-OCT). In TD-OCT, a scanning reference arm mirror is used, whereas in FD-OCT the reference arm mirror is fixed. In SD-OCT, a broadband laser source, and a spectrometer with a line camera are used, while in SS-OCT, a swept laser source and photodetector(s) are used. In SS-OCT, an in-depth profile (1D, known as an A-scan) of the sample is obtained by performing discrete Fourier transform on the acquired fringes recorded by the photodetector(s). Galvanometer mirrors added to the sample arm can be used to construct 2D (B-scan) and 3D (C-scan) images of the sample.

The optical properties of skin can vary significantly among individuals and over time, posing a challenge for absolute analyte level measurements. Thus, for the envisioned implantable glucose sensing biosensor, the micro-retroreflector-based platform must be self-calibrating. For example, one micro-retroreflector can be an analyte-responsive assay reflector while the remaining surrounding micro-retroreflectors can act as "always-on" reference reflectors, allowing for accurate determination of reflectivity reduction. Another requirement for the prospective implantable glucose sensing biosensor is the ability to detect and measure the signal in an automated regime. The unique and complex micro-retroreflector structures can act as an easily recognizable pattern when submerged in tissue. This approach will significantly simplify the future development of home products for blood glucose measurements.

In this paper, we report the first phase of creating such a biosensor that includes the development of the implantable solid platform, the employment of an imaging modality to detect and visualize the entire retroreflector pattern, and to monitor its reflectance in varying depths of highly scattering media, such as skin. For future phases of this study, we plan to integrate the necessary chemistry for the detection of specific analytes, such as glucose.

2. Materials and methods

2.1 Experimental setup

Figure 2 shows a schematic of a customized swept-source OCT (SS-OCT) system used in this study (based on Thorlabs SL1325, Newton, New Jersey, USA). A broadband swept-source laser with a wavelength of 1325 ± 50 nm and an output power of 12 mW was used as the optical source in this system. The A-line scanning rate was 16 kHz. The SS-OCT system was based on a Mach-Zehnder interferometer (MZI) where 10% of the power was directed to the reference arm and 90% to the sample arm. The interference fringes were detected by a balanced photodetector (Thorlabs PDB140C), which was used to remove the common mode noise, digitized using a 14-bit ADC (AlazarTech ATS460), and recalibrated using an MZI clock signal (MZI, Thorlabs INT-MZI-1300), which provided a frequency clock for the laser. The acquired images were 512 × 512 pixels. In-depth scanning was up to 3 mm (in air), while lateral scanning varied from 0.5 to 2 mm. The system's measured axial and transverse resolution were ~12 μm and ~15 μm (in air), respectively.

#130861 - $15.00 USD Received 29 Jun 2010; revised 23 Jul 2010; accepted 23 Jul 2010; published 2 Aug 2010

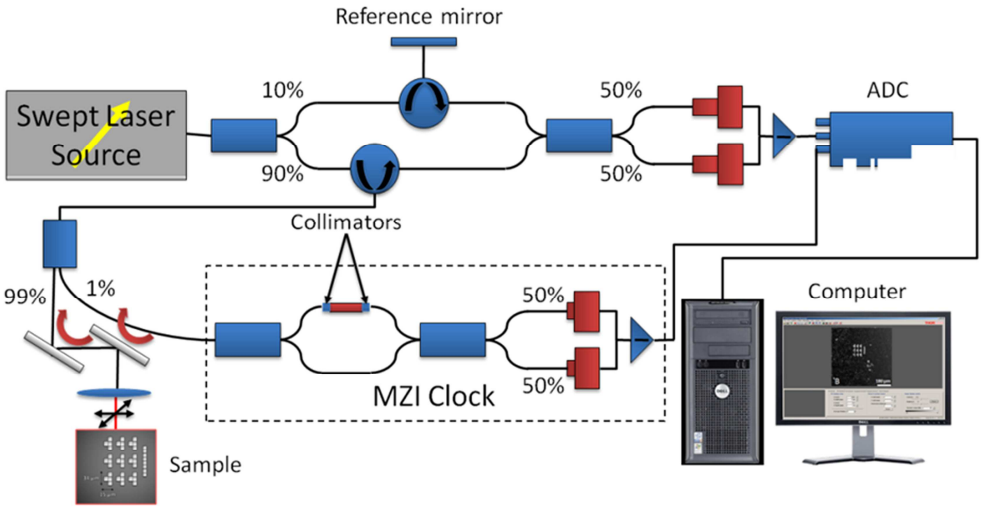

Fig. 2. The schematic outline of the SS-OCT system used in this study (ADC: analog to digital converter; MZI: Mach Zehnder interferometer).

2.2 Micro-retroreflectors

Linear micro-retroreflector arrays were fabricated as follows. A silicon wafer was coated with a 5 µm layer of polyimide, a 300 nm layer of poly(methyl glutarimide) (PMGI), and a 200 nm layer of poly(methyl-methacrylate) (PMMA) by spin-casting. The top PMMA layer was then exposed using electron beam lithography in the pattern of the retroreflectors, developed for 30 seconds in a 3:1 solution of isopropanol and methylisobutylketone, and rinsed in isopropanol. The PMGI layer was then etched in a 2.3% solution of tetramethyl ammonium hydroxide in water and a thin coating of nickel was then thermally evaporated onto the wafer surface. A lift-off step then dissolved the PMMA leaving only the nickel deposited in the resist openings. This pattern was further transferred into the polyimide by a directional oxygen reactive-ion etch. Finally, the entire structure was coated with a layer of gold. These structures were imaged with Scanning Electron Microscopy (SEM), and are shown in Fig. 3.

Micro-retroreflectors were 5 µm tall, 10 µm wide and 50 µm long. These linear micro-retroreflectors were designed to reflect light incident from any angle back to the source in an anti-parallel manner. The degree of alignment for linear micro-retroreflectors lies in one angular dimension, as shown in Fig. 1.

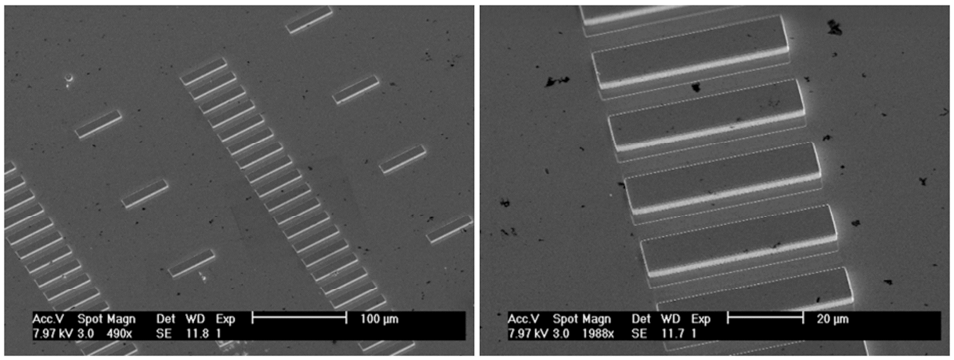

Fig. 3. SEM images of micro-retroreflector structures.

#130861 - $15.00 USD Received 29 Jun 2010; revised 23 Jul 2010; accepted 23 Jul 2010; published 2 Aug 2010

2.3 Sample preparation

Whole milk (with 3.7% fat content) and fresh porcine skin were used for testing SS-OCT imaging of micro-retroreflectors as a function of the scattering media depth. Porcine skin was purchased from the local market. Small skin samples (0.5 × 0.5 cm^2) were excised from the porcine ear and placed in a saline bath. The samples were kept hydrated while covering the micro-retroreflectors during SS-OCT imaging, and each sample was used only once.

3. Results

A silicon wafer containing gold micro-retroreflectors was mounted on top of a dual-axis rotating stage, which was further connected to a 2D-translational stage for 3D positioning. The focused incident light beam from the SS-OCT setup was directed onto the micro-retroreflectors and scanned over a 1 × 1 mm^2 area, an area sufficient for imaging the full micro-retroreflector array. At a 65° tilt angle, which provided maximum reflectivity for the fabricated micro-retroreflectors, 3D sample volumes were recorded by SS-OCT and reconstructed using LabVIEW and Thorlabs Swept 3D Viewer software. For each 3D volume, multiple rows of micro-retroreflectors were averaged together to create one 1D micro-retroreflector intensity profile. Figure 4A shows an example of a recorded 3D volume of micro-retroreflectors in air obtained after reconstruction of SS-OCT data, and Fig. 4B displays the average intensity profiles obtained within this 3D volume. The average intensity profile shown in Fig. 4B was constructed by averaging together each individual row of micro-retroreflectors displayed in Fig. 4A. B-scans were extracted from each 3D volume and peak analysis was performed. The retroreflectors were oriented with the scanning OCT beam such that scanning occurred parallel to the retroreflectors. This regime ensured the highest probability of equivalent reflectivity for all micro-retroreflectors.

To investigate the ability of SS-OCT to detect the entire micro-retroreflector pattern within scattering media as a function of depth, two sets of experiments were performed: one with whole milk and the other with porcine skin. In the first set of experiments, 21 different volumes of whole milk (with 3.7% fat content) were deposited, dropwise, on top of the micro-retroreflector array to provide different thicknesses of scattering medium. To prevent milk spillage, a plastic dam was designed and placed on the silicon wafer with adhesive glue. The varied depths of whole milk (refractive index, n = 1.35 [24],) were determined optically by SS-OCT after performing the experiments. Figure 5 represents typical one-dimensional micro-retroreflector intensity profiles for a selected set of samples with thicknesses ranging from 0.10 mm to 1.65 mm.

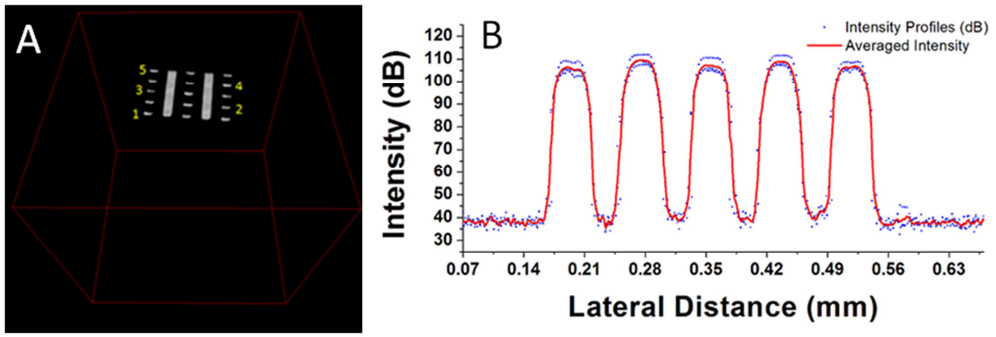

Fig. 4. (A) 3D volume (0.7 mm × 0.7 mm × 3 mm) of micro-retroreflectors in air obtained by SS-OCT with row indexing; (B) an averaged intensity profile of micro-retroreflectors in air (corresponding to an averaging through rows 1-5 of the micro-retroreflectors shown in A).

As expected, with an increase in sample depth the contrast between micro-retroreflectors and the background medium begins to decrease. Below the depth of 1.65 mm some micro-

#130861 - $15.00 USD Received 29 Jun 2010; revised 23 Jul 2010; accepted 23 Jul 2010; published 2 Aug 2010

retroreflectors become undetectable by SS-OCT, thereby, breaking the integrity of the entire platform pattern. One can see from this figure irregularities in uniformity of the selected peaks as the sample depth increases. This observation can be explained by the presence of inhomogeneities in whole milk, such as aggregates of fat globules and of protein particles [24]. Similar results were obtained for the remaining sets of samples, and are summarized in Fig. 6.

In the second set of experiments, a 0.5×0.5 cm^2 section of porcine skin was excised from porcine ear and placed in a saline bath to prevent dehydration and to preserve natural physiological conditions; 27 samples with thicknesses varying from 0.29 mm to 0.91 mm were used. Porcine tissue thicknesses were determined optically from SS-OCT images using the known refractive index (n = 1.45 [25],). Each sample was placed on top of the micro-retroreflectors, and 2D and 3D SS-OCT data sets were recorded. Figure 7 shows the micro-retroreflector intensity profiles for porcine tissue depths of 0.31 mm, 0.34 mm, 0.49 mm, 0.59 mm, 0.61 mm, and 0.80 mm.

In the case of porcine skin, below the depth of 0.91 mm some micro-retroreflectors become undetectable by SS-OCT. Figure 8 summarizes the contrast between micro-retroreflectors and porcine tissue for all samples studied in these experiments.

4. Discussion

The obtained results demonstrate the capability of SS-OCT to detect micro-retroreflectors within highly scattering media, such as whole milk and tissue, at depths up to at least 1.65 mm. With an increase in scattering media depth, the signal returning from the micro-retroreflectors decreases due to the attenuation of the photons. This reduces the contrast between the micro-retroreflectors and surrounding media. Here, we define contrast as the signal difference between micro-retroreflectors and media, excluding reflections returning from tissue inhomogeneities, when the entire platform pattern remains fully visible. The background signal (scattered photons from surrounding media) was averaged and subtracted from an averaged signal from the micro-retroreflector surface, which decreases with depth

#130861 - $15.00 USD Received 29 Jun 2010; revised 23 Jul 2010; accepted 23 Jul 2010; published 2 Aug 2010

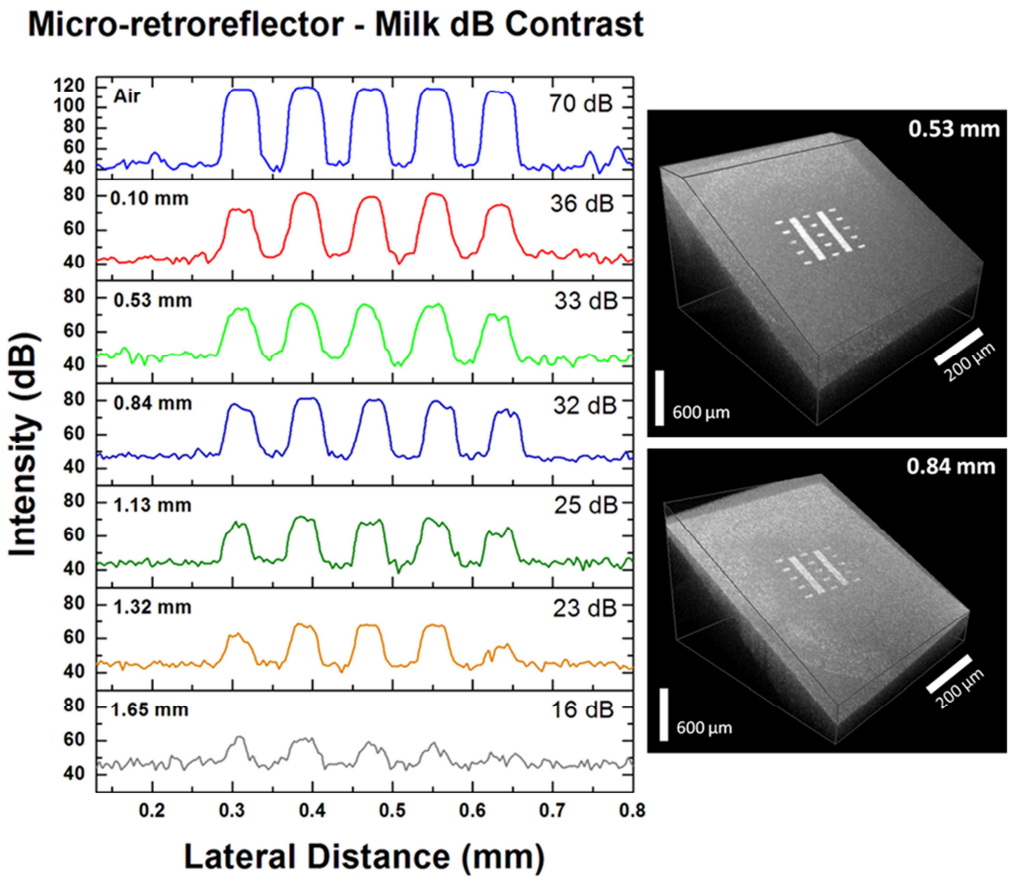

Fig. 5. Intensity profiles of micro-retroreflectors beneath varying depths of whole milk. Estimated dB contrast is shown in upper right corner of each pane. The 3D SS-OCT volumes (1 mm × 1 mm × 3 mm) on the right shows micro-retroreflectors beneath 0.53 mm and 0.84 mm of whole milk.

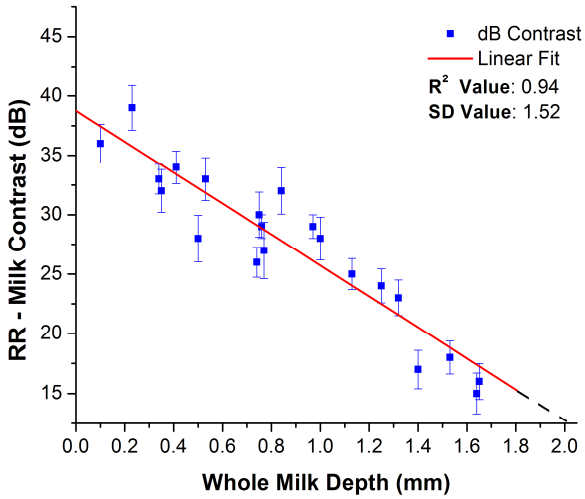

Fig. 6. Micro-retroreflector–milk contrast beneath varying depths of whole milk.

#130861 - $15.00 USD Received 29 Jun 2010; revised 23 Jul 2010; accepted 23 Jul 2010; published 2 Aug 2010

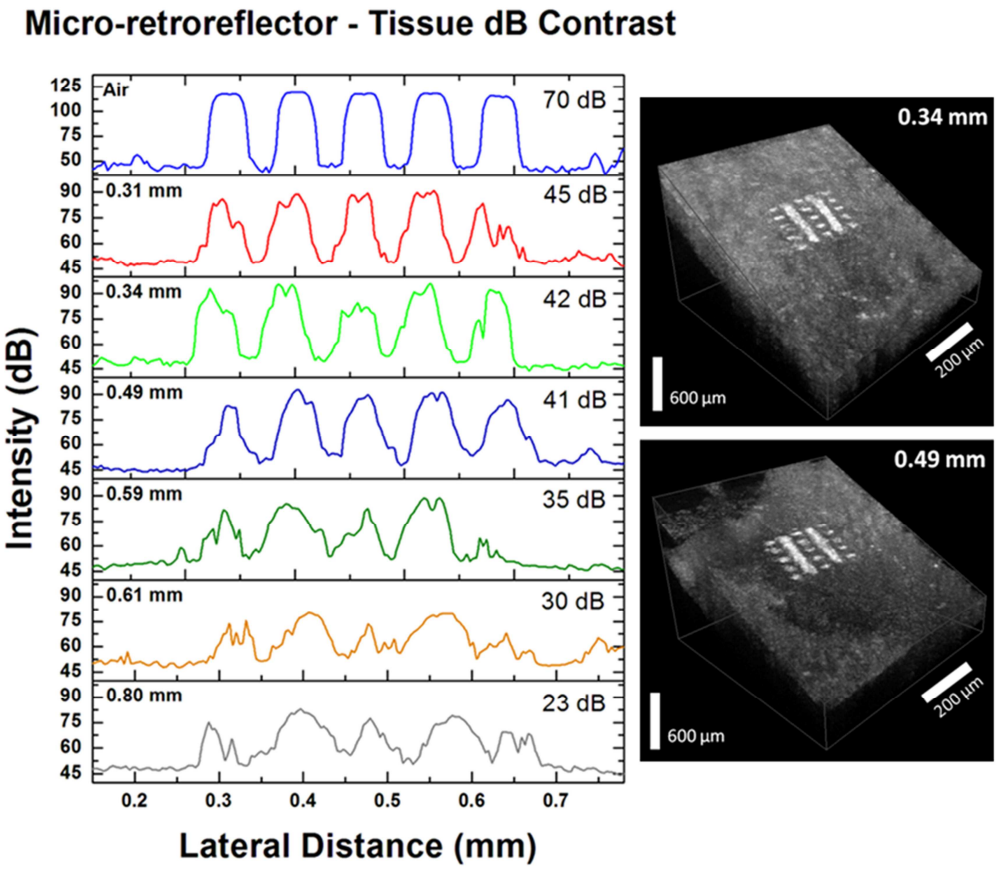

Fig. 7. Intensity profiles of micro-retroreflectors beneath varying thicknesses of porcine tissue. Estimated dB contrast is shown in upper right corner of each pane. The 3D SS-OCT volumes (1 mm × 1 mm × 3 mm) on the right show micro-retroreflectors beneath 0.34 mm and 0.49 mm of porcine tissue.

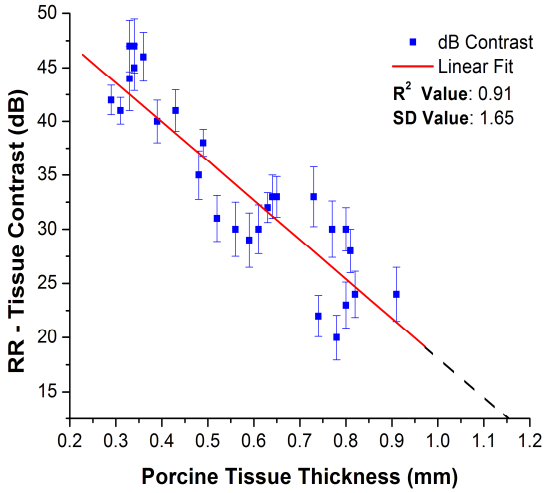

Fig. 8. Micro-retroreflector – tissue contrast beneath varying thicknesses of porcine tissue.

#130861 - $15.00 USD Received 29 Jun 2010; revised 23 Jul 2010; accepted 23 Jul 2010; published 2 Aug 2010

due to attenuation. A minimum level of contrast seen in this study was detected to be 15 ± 3.4 dB for whole milk and 20 ± 6.4 dB for porcine tissue. Below these levels, the micro-retroreflector structures were obstructed by tissue inhomogeneities. A maximum penetration depth of 2 mm for whole milk and 1.15 mm for porcine tissue was estimated by allowing the linear fit line in Fig. 6 and Fig. 8 to intercept the abscissa axis (where the contrast is close to 0 dB). From previous studies employing an analogous OCT setup it has been shown that approximate penetration depths achievable for porcine tissue is about 1 mm, which is in good accordance with our results [26].

Optical properties are different for homogeneous and heterogeneous media, and contrast between the micro-retroreflectors and surrounding media can vary greatly depending on the scattering nature of the media. Biological tissue can be described optically as a spatial distribution of refractive indices on the microscopic scale [27,28]. The local refractive index within the tissue can range from 1.34 to 1.50, depending on the type of biological tissue. This variation (mismatch) of refractive index distribution within the tissue can cause strong light scattering. On the other hand, whole milk can be described as a homogenous solution of scattering centers (fat aggregates and protein aggregates) with sizes ranging from the nanometer to sub-micrometer scale [24]. In contrast to whole milk, porcine tissue has a highly reflective rough surface and vast heterogeneity (tissue structures ranging from the micrometer to sub-millimeter scale) [26]. The necessity to maintain contrast above a certain level in order to distinguish the entire micro-retroreflector pattern from surrounding media reduces the maximum depth within which the micro-retroreflectors can be placed in different scattering media.

Overall, these results reveal the operational depths and potential contrast (micro-retroreflector – tissue) for the micro-retroreflector-based platform immersed in scattering media, such as biological tissue. It is important to reiterate that the operational depths for the envisioned platform are less than the known penetration depths achievable by OCT, due to necessity to provide complete pattern visibility. This therefore makes our work essential for understanding the depths at which the entire micro-retroreflector-based platform can be placed in highly scattering media before reflections are lost, which is necessary for the future development of micro-retroreflector based technologies that operate in the dermis tissue layer.

5. Conclusion

Our experimental results demonstrate the possibility of using OCT for the depth-resolved imaging and detection of micro-retroreflectors in skin, at depths reaching the dermis/subcutaneous fat layers. For this study, micro-retroreflectors were chosen because of their ability to direct incident light back to the detector in an anti-parallel manner. Incident light not directed onto the micro-retroreflectors will scatter in all directions with negligible amounts returning to the detector, thereby allowing for contrast to develop between the micro-retroreflectors and scattering medium. This characteristic makes imaging flat gold mirrors challenging, where it is required that the incident light beam be perpendicular to the sample surface in order to obtain maximal reflections. We have shown that the proposed micro-retroreflector-based platform can be detected with OCT at depths reaching 1.65 mm in whole milk and 0.91 mm in porcine tissue, which is generally less than maximum penetration depths achievable by OCT. This difference in depth is due to the necessity to provide sufficient contrast between the micro-retroreflector-based platform and surrounding scattering media. The minimum contrast was found to be 15 ± 3.4 dB for whole milk and 20 ± 6.4 dB for porcine tissue. High levels of minimum contrast for porcine tissue and whole milk are suggested to exist due to the presence of inhomogeneities in biological samples, which can obstruct the reflectivity of micro-retroreflector surfaces at greater depths. With further development of this assay platform, it may be possible to utilize OCT and micro-retroreflectors as a tool for monitoring glucose levels and other analytes in subcutaneous tissue environments by decorating the micro-retroreflector surface with chemical compounds

#130861 - $15.00 USD Received 29 Jun 2010; revised 23 Jul 2010; accepted 23 Jul 2010; published 2 Aug 2010

selectivity sensitive to certain analytes, which can then alter surface reflectivity due to changes in analyte concentration.

Acknowledgements

This study was supported by a grant from the National Science Foundation (CMMI-0900743 to Dr. Kirill Larin, Dr. Paul Ruchhoeft, and Dr. Richard Willson), and by a grant from the Welch Foundation (E-1264) to Dr. Richard Willson. Furthermore, the project described was supported by Grant Number U54 AI057156 from NIAID/NIH. Its contents are solely the responsibility of the authors and do not necessarily represent the official views of the RCE Programs Office, NIAID, or NIH. Finally, we thank Narendran Sudheendran, Ravi Kiran Manapuram, and Venu Gopal Reddy Manne for their help with experiments, data processing, and discussion of the data.

#130861 - $15.00 USD Received 29 Jun 2010; revised 23 Jul 2010; accepted 23 Jul 2010; published 2 Aug 2010